4
Electromechanical system with internal impacts and uncertainties

The system analyzed in this chapter is composed by a cart whose motion is driven by a DC motor, sketched in Fig. 2.1, and a embarked pendulum into this cart. The motor is coupled to the cart through a pin that slides into a slot machined on an acrylic plate that is attached to the cart, as shown in Fig. 4.1. The off-center pin is fixed on the disc at distance Δ of the motor shaft, so that the motor rotational motion is transformed into a cart horizontal movement. The suspension point of the pendulum is fixed in the cart, so that exists a relative motion between cart and pendulum induced by the motion of the cart. The embarked pendulum is modeled as a mathematical pendulum (bar without mass and particle of mass m_p at the end). The pendulum length is represented by l_p and the pendulum angular displacement by θ. The mass of the mechanical system, m, is equal the cart mass plus pendulum mass, m_c+m_p. The horizontal cart position is represented by x. Due to constraints, the cart is not allowed to move in the vertical direction. A flexible barrier is attached inside the cart, constraining the pendulum motion. Due to the relative motion between the cart and the pendulum, it is possible that occur impacts between the pendulum and the barrier, as suggested in Fig. 4.1. As the impacts are internal, the energy

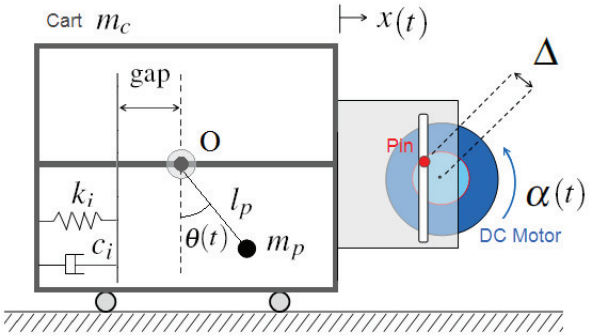

Figure 4.1: Coupled motor-cart-pendulum-barrier system.

stored in the pendulum motion it is not transferred outside the system, it stays within, with a possible dissipation. This system configuration helps to understand the difference between an internal and an external barrier. The objective is to analyze the maximal energy stored in the barrier in impacts as function of some parameters of the electromechanical system. Due to the presence of uncertainties in the computational nonlinear dynamics model of the

electromechanical system, the energy analysis is performed from a stochastic view point for different levels of uncertainties, and also for the deterministic case.

In the deterministic analysis, these parameters are the horizontal distance from the suspension point of the pendulum to the equilibrium position of the barrier and the coupling parameter between motor and the mechanical system, Δ. Numerical simulations were performed with different values of these parameters. The coupling parameter has been varied from zero, an asymptotic case, (meaning no coupling between motor and the mechanical system) up to 10^{-3} m. Comparing the results obtained with $\Delta = 0$ and with $\Delta > 0$, it is possible to observe the influence of the coupling in the maximal energy stored in the barrier.

4.1 Dynamics of the motor-cart-pendulum-barrier system

A continuous contact dynamic model is developed and the impact is described using the spring-dashpot model. The spring-damper element of the impact is represented by a spring with stiffness k_i and a damper with damping coefficient c_i. The equations of the cart-pendulum-barrier system were obtained with the Lagrange principle. They are

$$m_p l_p^2 \ddot{\theta}(t) + m_p l_p \ddot{x}(t) \cos\theta(t) + m_p g_a l_p \sin\theta(t) = f_{\text{imp}}(t) l_p \cos\theta(t)\,, \tag{4.1}$$

$$(m_p + m_c)\ddot{x}(t) + m_p l_p \ddot{\theta}(t) \cos\theta(t) - m_p l_p \dot{\theta}^2(t) \sin\theta(t) = f(t)\,, \tag{4.2}$$

where, g_a is the acceleration of gravity, f represents the horizontal coupling force between the DC motor and the cart and f_{imp} the impact force exerted in the pendulum. This force is written as:

$$f_{\text{imp}}(t) = -\phi(t) \left[k_i \left(l_p \sin\theta(t) + \text{gap} \right) + c_i \left(l_p \dot{\theta}(t) \cos\theta(t) \right) \right], \tag{4.3}$$

$$\phi(t) = \begin{cases} 1\,, & if \quad -l_p \sin\theta(t) > \text{gap}\,, \\ 0\,, & if \quad -l_p \sin\theta(t) \leq \text{gap}\,, \end{cases} \tag{4.4}$$

in Eq. (4.4) gap is the horizontal distance from the suspension point to the equilibrium position of the barrier. Due to the system geometry, $x(t)$ and $\alpha(t)$ are related by the following constraint

$$x(t) = \Delta \cos\alpha(t)\,. \tag{4.5}$$

Substituting Eqs. (2.6) and (4.1) to (4.5) into Eqs. (2.1) and (2.2), we obtain the initial value problem for the motor-cart-pendulum-barrier system. Given

a constant source voltage ν, find (α, c, θ) such that, for all $t > 0$,

$$l\dot{c}(t) + rc(t) + k_e\dot{\alpha}(t) = \nu\,,$$

$$\begin{aligned}&\ddot{\alpha}(t)\left[j_m + (m_c + m_p)\Delta^2(\sin\alpha(t))^2\right] + \dot{\alpha}(t)\left[b_m + (m_c + m_p)\Delta^2\dot{\alpha}(t)\cos\alpha(t)\ \sin\alpha(t)\right]\\ &\quad -k_e\ c(t)\ -\ \ddot{\theta}(t)\left[m_p l_p\cos\theta(t)\Delta\sin\alpha(t)\right] + \dot{\theta}(t)\left[m_p\ l_p\dot{\theta}(t)\sin\theta(t)\Delta\sin\alpha(t)\right] = 0\,,\end{aligned}$$

$$\begin{aligned}&\ddot{\theta}(t)\left[m_p\ l_p^2\right] - \ddot{\alpha}(t)\left[m_p\ l_p\ \cos\theta(t)\Delta\sin\alpha(t)\right] -\ \dot{\alpha}(t)\left[m_p\ l_p\cos\theta(t)\Delta\cos\alpha(t)\dot{\alpha}(t)\right]\\ &\quad + m_p\ g_a\ l_p\sin\theta(t) + \phi(t)\left[k_i(l_p\sin\theta(t) + \text{gap}) + c_i(l_p\dot{\theta}(t)\cos\theta(t))\right] l_p\cos\theta(t) =\ 0\,,\end{aligned} \tag{4.6}$$

where

$$\phi(t) = \begin{cases} 1, & \text{if} \quad -l_p\sin\theta(t) > \text{gap}\,,\\ 0, & \text{in all other cases}\,,\end{cases} \tag{4.7}$$

with the initial conditions,

$$\dot{\alpha}(0) = 0 \quad , \quad \alpha(0) = 0 \quad , \quad \dot{\theta}(0) = 0 \quad , \quad \theta(0) = \pi/2 \quad , \quad c(0) = \frac{\nu}{r}\,. \tag{4.8}$$

4.2 Dimensionless motor-cart-pendulum-barrier system

In this section, the initial value problem to the motor-cart-pendulum-barrier system is presented in a dimensionless form. Taking $\dot{\alpha}(t) = u(t)$ and $\dot{\theta}(t) = n(t)$, the system can be written as a first order system

$$\dot{c}(t) = \ \frac{-k_e u(t) - rc(t) + \nu}{l}\,,$$

$$\begin{aligned}\dot{u}(t) = \ &\{-n(t)^2 m_p l_p\sin\theta(t)\Delta\sin(\alpha(t)) - u(t)^2(m_c + m_p)\Delta^2\cos(\alpha(t))\sin(\alpha(t))\\ &-b_m u(t) + k_e c(t) + [\cos(\theta(t))\Delta\sin(\alpha(t))]\,[u(t)^2 m_p\cos\theta(t)\Delta\cos\alpha(t)\\ &-m_p g_a\sin(\theta(t)) - \phi\,[k_i(l_p\sin\theta(t) + \text{gap}) + c_i(l_p n(t)\cos\theta(t))]\cos\theta(t)\ ]\ \}\\ &\left\{\frac{1}{j_m + \Delta^2\sin(\alpha(t))^2(m_c + m_p\sin(\theta(t))^2)}\right\}\,,\end{aligned}$$

$$\begin{aligned}\dot{n}(t) = \ &\{m_p\cos(\theta(t))\Delta\sin(\alpha(t))\,[k_e c(t) - u(t)^2(m_c + m_p)\Delta^2\cos(\alpha(t))\sin(\alpha(t))\\ &-b_m u(t) - n(t)^2 m_p l_p\sin\theta(t)\Delta\sin(\alpha(t))\ ] + \left[j_m + (m_p + m_c)\Delta^2\sin(\alpha(t))^2\right]\\ &[-m_p g_a\sin(\theta(t)) + u(t)^2 m_p\cos\theta(t)\Delta\cos\alpha(t) - \phi\,[k_i(l_p\sin\theta(t) + \text{gap})\\ &+c_i(l_p n(t)\cos\theta(t))\ ]\cos\theta(t)\ ]\ \}\\ &\left\{\frac{1}{m_p l_p\left[j_m + \Delta^2\sin(\alpha(t))^2(m_c + m_p\sin(\theta(t))^2)\right]}\right\}\,.\end{aligned} \tag{4.9}$$

Writing

$$t = \frac{l}{r}s, \quad \alpha\left(\frac{l}{r}s\right) = \gamma(s), \quad u\left(\frac{l}{r}s\right) = \frac{rq(s)}{l}, \quad \theta\left(\frac{l}{r}s\right) = \beta(s),$$
$$n\left(\frac{l}{r}s\right) = \frac{ry(s)}{l}, \quad c\left(\frac{l}{r}s\right) = \frac{k_e w(s)}{l}, \tag{4.10}$$

one gets that s is dimensionless parameter. The functions $\gamma(s)$, $q(s)$, $\beta(s)$, $y(s)$ and $w(s)$ are dimensionless functions. By substituting Eq. (4.10) into Eq. (4.9) one obtains

$$w'(s) = \; -w(s) - q(s) + v_0 \;,$$

$$\begin{aligned} q'(s) = \; & \{-v_3 q(s) - y(s)^2 v_5 \sin(\gamma(s)) \sin(\beta(s)) - v_6 \sin(\beta(s)) \cos(\beta(s)) \sin(\gamma(s)) \\ & + v_2 w(s) - q(s)^2 \cos(\gamma(s)) \sin(\gamma(s)) \left[v_9 - v_4 \cos(\beta(s))^2\right] \\ & - \varphi(s) \cos(\beta(s))^2 \sin(\gamma(s)) \left[v_{10} \sin(\beta(s)) + v_{11} + v_{12} \cos(\beta(s)) y(s)\right] \} \\ & \left\{ \frac{1}{1 + \sin(\gamma(s))^2 \left[v_1 + v_4 \sin(\beta(s))^2\right]} \right\} \end{aligned} \tag{4.11}$$

$$\begin{aligned} y'(s) = \; & \{-v_3 v_7 q(s) \cos(\beta(s)) \sin(\gamma(s)) + q(s)^2 v_7 \cos(\gamma(s)) \cos(\beta(s)) \\ & - v_4 y(s)^2 \sin(\gamma(s))^2 \sin(\beta(s)) \cos(\beta(s)) + v_2 v_7 w(s) \cos(\beta(s)) \sin(\gamma(s)) \\ & \left[1 - v_9 \sin(\gamma(s))^2\right] \left[-v_8 \sin(\beta(s)) - \varphi(s)(v_{13}(\sin(\beta(s)) + v_{14}) \right. \\ & \left. + v_{15} y(s) \cos(\beta(s))) \cos(\beta) \right] \} \left\{ \frac{1}{1 + \sin(\gamma(s))^2 \left[v_1 + v_4 \sin(\beta(s))^2\right]} \right\} , \end{aligned} \tag{4.12}$$

where

$$\varphi(s) = \begin{cases} 1 \;, & if \quad -\sin\beta(s) > a_{14} \;, \\ 0 \;, & if \quad -\sin\beta(t) \leq a_{14} \;, \end{cases} \tag{4.13}$$

and where $'$ denotes the derivative with respect to s and a_i, $i = 1, \cdots, 16$ are dimensionless parameters given by

$$\begin{aligned} & v_0 = \frac{\nu l}{k_e r}, \quad v_1 = \frac{\Delta^2 m_c}{j_m}, \quad v_2 = \frac{l k_e^2}{j_m r^2}, \quad v_3 = \frac{b_m l}{j_m r}, \quad v_4 = \frac{\Delta^2 m_p}{j_m}, \\ & v_5 = \frac{m_p l_p \Delta}{j_m}, \quad v_6 = \frac{m_p \Delta g_a l^2}{j_m r^2}, \quad v_7 = \frac{\Delta}{l_p}, \quad v_8 = \frac{g_a l^2}{l_p r^2}, \quad v_9 = \frac{(m_c + m_p)\Delta^2}{j_m}, \\ & v_{10} = \frac{k_i l_p \Delta l^2}{j_m r^2}, \quad v_{11} = \frac{k_i \text{gap} \Delta l^2}{j_m r^2}, \quad v_{12} = \frac{c_i l_p \Delta l}{j_m r}, \quad v_{13} = \frac{k_i l^2}{m_p r^2}, \quad v_{14} = \frac{\text{gap}}{l_p}, \\ & v_{15} = \frac{c_i l}{m_p r}. \end{aligned} \tag{4.14}$$

Comparing the dimensionless parameters of the motor-cart-pendulum-barrier system with the dimensionless parameters of the motor-cart-pendulum system given by Eq. 3.9, it can be observed that the internal barrier introduces six news parameters to the equations: v_{10} to v_{15}.

4.3 Impact energy

As explained in the introduction, the objective of this chapter is to analyze the maximum energy stored in the barrier in each impact in function of some parameters of the electromechanical system. These parameters are gap $/l_p$ and Δ. The maximum impact energy during the j-th impact, λ_j, occurs when the spring k_i is compressed to the maximum, that is, when $l_p \sin(\theta)$ achieves its minimum value during the j-th impact. Noting as $\theta^\star$ the angle of the pendulum corresponding to this configuration of maximum compression, λ_j is calculated by

$$\lambda_j = \frac{1}{2} k_i \left(l_p \sin(\theta^\star) + gap\right)^2, \qquad \text{with} \quad -l_p \sin\theta^\star > \text{gap} \ . \tag{4.15}$$

The average of the maximum impact energy is written as

$$\lambda = \frac{\sum_{j=1}^{N_{\text{imp}}} \lambda_j}{N_{\text{imp}}} \ , \tag{4.16}$$

where N_{imp} is the total number of impacts that occur during time interval $[0, T]$. T is the duration chosen for analysis. The variable λ is chosen to measure the system performance. The bigger λ is, the better will be the system performance.

4.4 Numerical simulations of the dynamics of the coupled system

To observe the influence of the coupling between the electrical and mechanical parts in the maximum energy stored in the barrier, two configurations of the vibro-impact system were analyzed separately. In the first one, it is considered no coupling between the motor and the mechanical system, i.e., $\Delta = 0$ m. In this case, the motor behaves as if it is turned off and, consequently, the cart does not move. In the second configuration, it is considered coupling, i.e., $\Delta > 0$ m.

4.4.1 No coupling between the motor and the mechanical system

When $\Delta = 0$ m, there is no coupling between the motor and the mechanical system. Thus the cart does not move. Considering that there is no energy dissipation in the impact model between the pendulum and the barrier ($c_i = 0$ Ns/m), the maximum energy stored in the barrier in each impact can be calculated as function of the initial potential and kinetic energies of the pendulum. Calling the initial conditions for the pendulum as $\theta(0) = \theta_0$ and $\dot{\theta}(0) = \dot{\theta}_0$, the initial mechanical energy of the pendulum is

$$\lambda_0 = m_p\ g\ \cos(\theta_0) + \frac{1}{2} m_p[(l_p\dot{\theta}_0 \cos\theta_0)^2 + (l_p\dot{\theta}_0 \sin\theta_0)^2]\,. \tag{4.17}$$

When the spring k_i is compressed to the maximum during the j-th impact, a part of λ_0 is stored as potential energy in the pendulum and another part as potential energy in spring k_i (λ_j). Thus

$$\lambda_0 = m_p\ g\ \cos(\theta^\star) + \frac{1}{2} k_i\ (l_p \sin(\theta^\star) + gap)^2\,. \tag{4.18}$$

Observing Eq. (4.17), it is possible to verify that when $\Delta = 0$ m, λ_j the j-th impact will be maximum if $\text{gap}/l_p = 0$. With this configuration, the pendulum begins the impact in the vertical position, exactly when it has its maximum velocity. Thus, this configuration is taken as reference. The impact energy in this configuration represented by λ^{ref} will be used as normalization factor in the analysis of the impact factor. The value of λ^{ref} is computed considering $k_i = 10^6$ N/m. The graph of λ/λ^{ref} as function of gap/l_p for different values of k_i is shown in Fig. 4.2. As expected, its maximum occurs when $\text{gap}/l_p = 0$ and its minimum at $\text{gap}/l_p = 1$ (configuration in which there is no impact between the pendulum and the barrier).

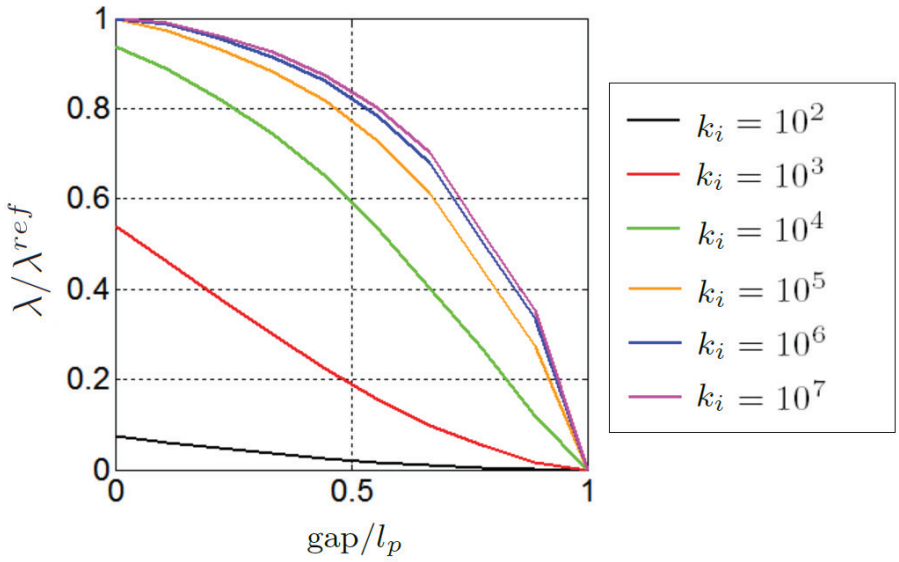

Figure 4.2: No coupling ($\Delta = 0$ m): normalized average of the maximum impact energy as function of the parameter gap/l_p for different values of k_i N/m.

4.4.2 Coupled system

When $\Delta > 0$ m, i.e., there is coupling between the motor and the mechanical system. The bigger is Δ, the more highlighted will be the non-linear behavior of system [42]. Small changes in the values of Δ and gap/l_p can modify a lot the response of the system, as the maximum amplitude

of the pendulum displacement, maximum velocity of the motor shaft and therefore, the impact behavior of the system. The form of the graph of the average of the impact energy changes as shown in Sec. 4.4. Considering just the coupled motor-cart system, i.e., there is no pendulum embarked in the cart, the existence and asymptotic stability of a periodic orbit were already obtained in a mathematically rigorous way in [15, 18]. The influence of the parameters Δ and gap/l_p in λ, Eq. (4.16), was investigated numerically. For computation, the initial value problem defined by Eqs. (4.6) to (4.8) has been rewritten in the dimensionless form given by Eqs. (4.11) to (4.14). Despite of using the dimensionless initial value problem for numerical simulations, the results are presented in the dimensional form because we believe that in this way they have an easier physical interpretation. Duration is chosen as $T = 20.0$ s. The 4th-order Runge-Kutta method is used for the time-integration scheme. The specifications of the motor parameters used in all simulations were obtained from the specifications of the DC motor Maxon brushless number 411678 (values could be find at [42](table 1)). The applied voltage was assumed to be constant in time and equal to 2.4 V. The pendulum length was assumed to be 0.075 m. The values of the cart and the pendulum masses were $m_c = 0.0$ kg and $m_p = 5.0$ kg, so that the total mass, $m = m_c + m_p = 5.0$ kg, is equal to the embarked mass, a limit case. The values of the stiffness and damping coefficient used in the simulations were $k_i = 10^6$ N/m and $c_i = 0$ Ns/m, so that there is no energy dissipation in the impact model. To investigate the influence of Δ and gap/l_p in λ/λ^{ref}, 700 numerical simulations have been carried out combining the following values of the parameters: 7 values for Δ nonuniformly selected in the interval $[0\,, 10^{-3}]$ m, and 100 values for gap/l_p uniformly selected in $[0\,, 1]$. Figure 4.3 shows the graph of λ/λ^{ref} as function of gap/l_p for different values of Δ. It is noted that for values of d near zero, as 10^{-5} m and 10^{-4} m, the graph of the impact energy is very similar to the graph with $\Delta = 0$ m. The average impact energy presents its maximum at $\text{gap}/l_p = 0$ and its minimum when $\text{gap}/l_p = 1$. When Δ is bigger, as 2×10^{-4} m, 5×10^{-4} m, 8×10^{-4} m and 10^{-3} m, the form of the graph of the average of the impact energy changes completely. The maximum does not occur anymore at $\text{gap}/l_p = 0$. Depending on the value of Δ, the maximum occurs at a different value of gap/l_p. Among the considered values of Δ and gap/l_p, the maximum of the average of the impact energy was obtained with $\Delta = 10^{-3}$ m and $\text{gap}/l_p = 0.6263$. Considering $\Delta = 10^{-3}$ m and varying the value of k_i, the shape of the curve of the average of the maximum impact energy in function of the parameter gap/l_p (shown in Fig. 4.4) changes in an unexpected fashion. Comparing it with Fig. 4.3, it is possible to observe that for small values of

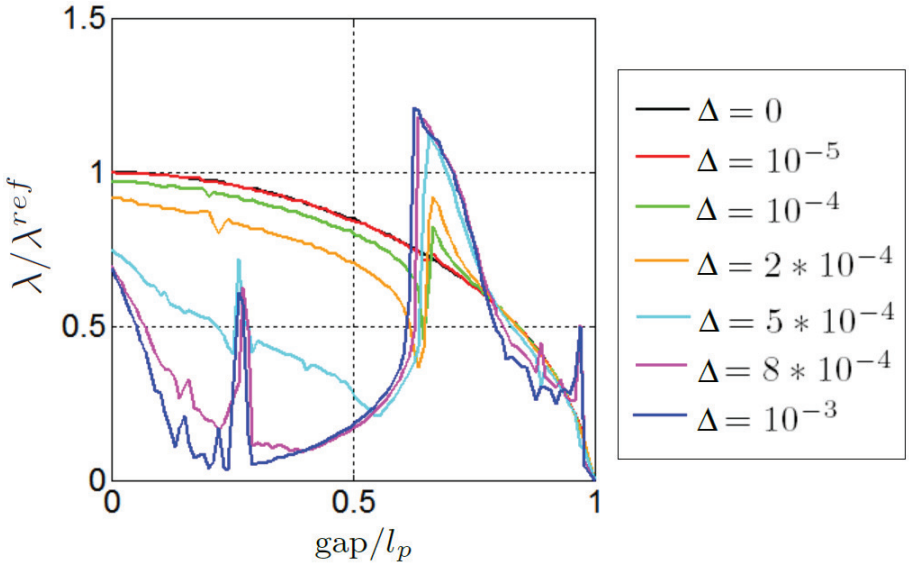

Figure 4.3: Coupled system ($\Delta > 0$): normalized average of the impact energy as function of the parameter gap/l_p for different values of Δ (units in meters).

k_i, as 10^2 N/m and 10^3 N/m, both graphs are similar. But, when k_i is bigger, the form of the graph of the average of the impact energy changes completely. Among the considered values of k_i and gap/l_p, the maximum of the average of the impact energy was obtained with $k_i = 10^4$ N/m and gap/$l_p = 0.293$. Thus the maximum of the average of the impact energy does not occur anymore with the bigger k_i as happens in the $\Delta = 0$ m configuration. To construct the graph of Fig. 4.4, for each value of k_i selected, 100 values of gap/l_p equally spaced between 0 and 1 were considered. Thus, in total, 600 numerical simulations have been carried out.

4.5 Probabilistic model

The system parameter considered uncertain is k_i, which is modeled by the random variable K_i. The probability distribution of this random variable is constructed using the Maximum Entropy Principle [34, 88, 89, 91, 85, 94, 95]. This Principle allows the probability distribution of a random variable to be constructed using only the available information, avoiding the use of any additional information that introduces a bias on the estimation of the probability distribution. The Maximum Entropy Principle states: out of all probability distributions consistent with a given set of available information choose the one that has maximum uncertainty (the Shannon measure of entropy). The available information of the random variable is defined as

1. K_i is a positive-valued random variable,

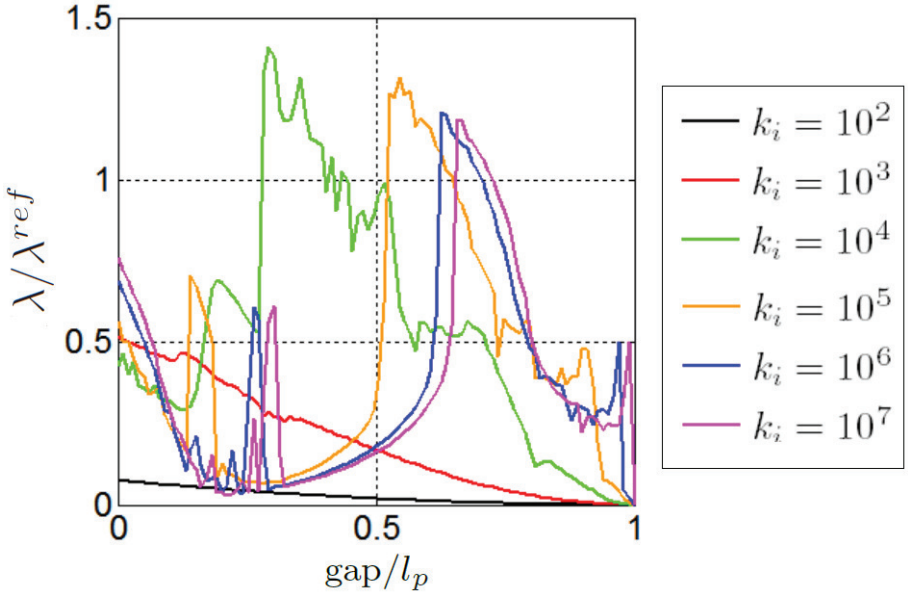

Figure 4.4: Coupled system ($\Delta > 0$): normalized average of the impact energy as function of the parameter gap/l_p for different values of k_i N/m with $\Delta = 10^{-3}$ m.

2. the mean value is known: $E\{K_i\} = \mu$,

3. in order that the response of the dynamical system be a second-order stochastic process, we impose the following condition: $\|E\{\log K_i\}\| < \infty$.

Therefore, the Maximum Entropy Principle using Shannon entropy measure of the probability density function, p, of K_i yields the Gamma probability density function, given by

$$p(k_i) = \mathbb{1}_{[0,+\infty)}(k_i)\,\frac{1}{\mu}\left(\frac{1}{\delta^2}\right)^{\frac{1}{\delta^2}}\frac{1}{\Gamma(1/\delta^2)}\left(\frac{x}{\mu}\right)^{\frac{1}{\delta^2}-1}\exp\left(\frac{x}{\delta^2\mu}\right)\,, \tag{4.19}$$

where $\mathbb{1}_{[0,+\infty)}(k_i)$ is an indicator function that is equal to 1 for $k_i \in [0,+\infty)$ and 0 otherwise, and

- Γ is the Gamma function: $\Gamma(a) = \int_0^\infty t^{a-1}\exp(-t)\mathrm{d}t$;
- $\delta = \frac{\sigma}{\mu}$ is the coefficient variation (σ is the standard deviation).

4.6 Numerical simulations of the stochastic vibro-impact electromechanical system

As it was assumed that the stiffness of the spring, k_i, in the barrier model is a random variable, the output variables of the stochastic coupled system are random processes [91, 11] and, consequently, the average of the impact energy,

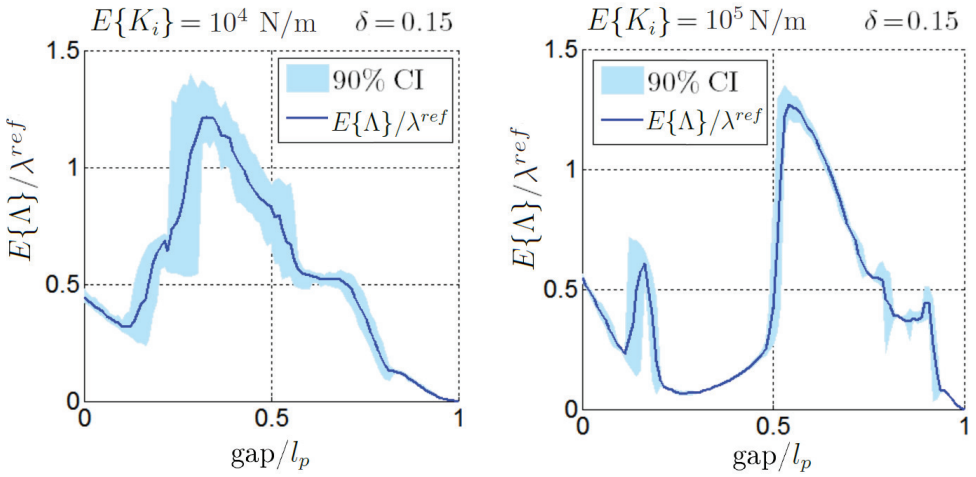

4.5(a): 4.5(b):

Figure 4.5: Mean and 90% confidence interval of Λ/λ^{ref} as function of gap/l_p with $\delta = 0.15$ for(a) $E\{K_i\} = 10^4$ N/m and (b)$E\{K_i\} = 10^5$ N/m .

λ, become a random variable Λ. To make the stochastic analysis, Monte Carlo simulations were employed to compute statistics of Λ, as mean and intervals of confidence, using 100 independent realizations of K_i. To observe the influence of gap/l_p in the statistics of the impact energy for different values of $E\{K_i\}$ and hyperparameter δ (which controls the level of uncertainties for K_i), the Monte Carlo simulations have been carried out combining the following values of the parameters: 3 values for $E\{K_i\}$ (10^4, 10^5, and 10^6 N/m), 3 values for δ (0.15, 0.25, and 0.35) and 100 values for gap/l_p uniformly selected in the interval $[0\,, 1.0]$. Thus, $90,000$ numerical simulations have been carried out in the stochastic analysis. The graphs of $E\{\Lambda\}/\lambda^{ref}$ and 90% confidence interval as function of gap/l_p for $E\{K_i\} = 10^4$, 10^5 and 10^6 N/m with $\delta = 0.15$ are displayed in Figs. 4.5 and 4.6(a). Comparing these statistics with the results of deterministic simulations shown in Fig. 4.4, it is verified that in relation to the impact energy, deterministic and stochastic systems have similar behavior. However, the 90% confidence interval gets narrower as $E\{K_i\}$ increases. For $E\{K_i\} = 10^6$ N/m and $\delta = 0.15$, the maximum of $E\{\Lambda\}/\lambda^{ref}$ occurs at gap/l_p = 0.63 m. The normalized histogram of Λ/λ^{ref} with this configuration is shown in Fig. 4.6(b). Figures 4.7 to 4.9 show the graphs of $E\{\Lambda\}/\lambda^{ref}$ and 90% confidence interval as function of gap/l_p for $E\{K_i\} = 10^4$, 10^5 and 10^6 N/m and for $\delta = 0.25$ and 0.35. These figures show that the bigger δ is, the larger is the confidence interval of Λ/λ^{ref}.

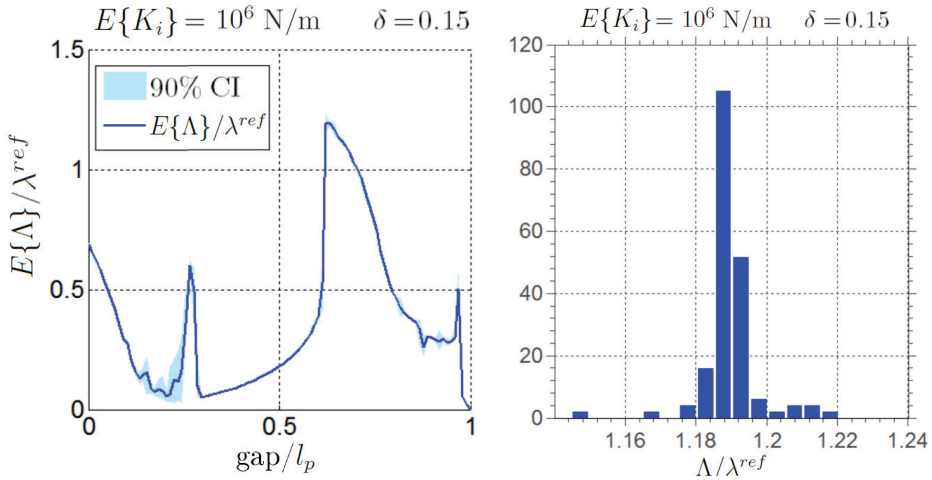

4.6(a): 4.6(b):

Figure 4.6: (a) Mean and 90% confidence interval of Λ as function of gap/l_p with $\delta = 0.15$ and $E\{K_i\} = 10^6$ N/m and (b) normalized histogram of Λ/λ^{ref} for gap/$l_p = 0.63$ m, $E\{K_i\} = 10^6$ N/m and $\delta = 0.15$.

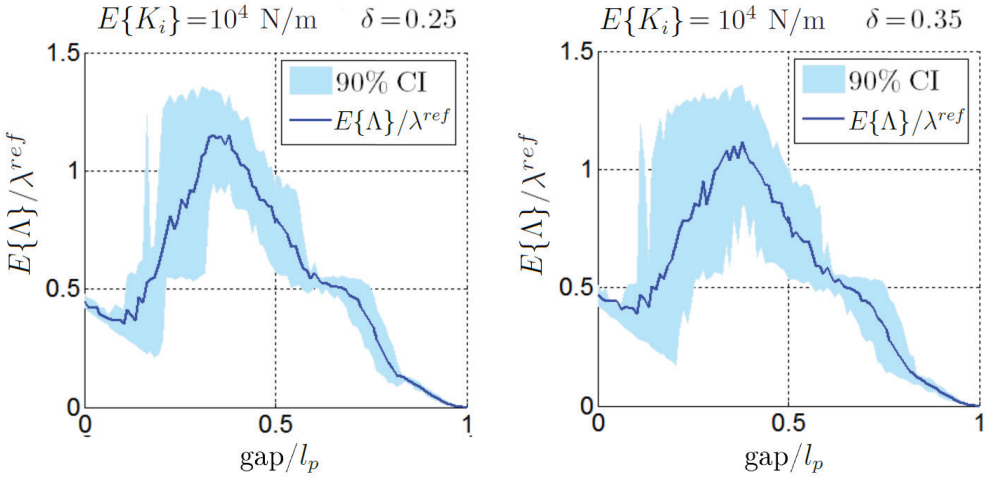

4.7(a): 4.7(b):

Figure 4.7: Mean and 90% confidence interval of Λ/λ^{ref} as function of gap/l_p with $E\{K_i\} = 10^4$ N/m for(a) $\delta = 0.25$ and (b) $\delta = 0.35$.

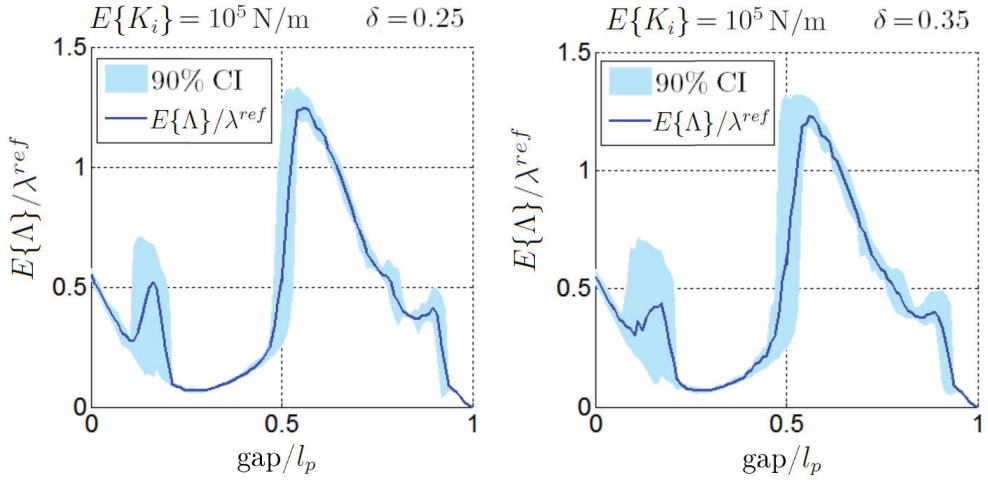

4.8(a): 4.8(b):

Figure 4.8: Mean and 90% confidence interval of Λ/λ^{ref} as function of gap/l_p with $E\{K_i\} = 10^5$ N/m for(a) $\delta = 0.25$ and (b) $\delta = 0.35$.

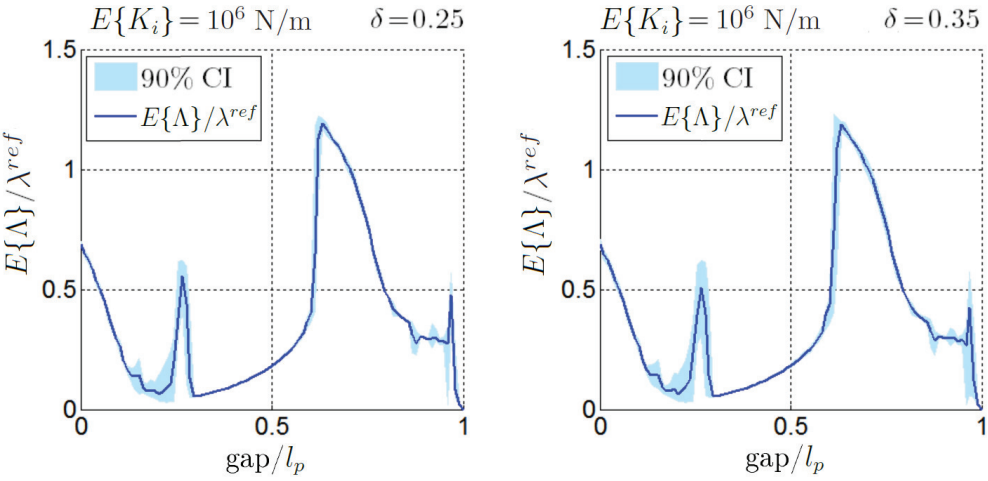

4.9(a): 4.9(b):

Figure 4.9: Mean and 90% confidence interval of Λ/λ^{ref} as function of gap/l_p with $E\{K_i\} = 10^6$ N/m for(a) $\delta = 0.25$ and (b) $\delta = 0.35$.

4.7 Summary of the Chapter

The purpose of this chapter was to analyze the impact energy of an embarked pendulum in a vibro-impact electromechanical system. A flexible barrier, attached to the cart, constrains the pendulum motion and causes impacts. Since this nonlinear electromechanical system is devoted to the vibro-impact, the time responses exhibit numerous shocks that have to be identified with accuracy and, consequently, a very small time-step is required. To reduce the computation time, the initial-value problem, Eqs. (4.6) to (4.8), was rewritten in the dimensionless form, Eqs. (4.11) to (4.13). While each numerical simulation of Eqs. (4.6) to (4.8) takes approximately 30 seconds to be computed, each numerical simulation of Eqs. (4.6) to (4.8) takes approximately half of this time. In the deterministic analysis, the influence of the parameter gap$/l_p$ in the impact behavior was numerically investigated for different values of the nominal eccentricity of the pin, Δ, the parameter that governs the coupling and the nonlinearity of the system. As Δ increases the nonlinearity also increases. It was verified that for values of Δ near zero, the graph of the impact energy is very similar to the graph with $\Delta = 0$ m. This result can be nicely predicted from conservation of energy. However, as Δ increases the form of the graph changes completely and in an unexpected fashion. This peculiar behavior is due to the energy taken by the pendulum from the motor. The energy of the mechanical systems varies a lot and the pumping of energy, from the motor to the mechanical system, increases with Δ. The systems analyzed show a self-oscillation behavior, in the sense that the generation and maintenance of the motion comes from the motor but the oscillations somehow control the energy taken from the motor. It varies with Δ, that is a measure of the nonlinearity of the system. It is worth mentioning that the energy intake is at frequency zero, the constant voltage, but this energy is distributed to all frequencies due to the impacts. The influence of the parameter gap$/l_p$ in the impact behavior was also investigated for different values of the stiffness, k_i, with the fixed value $\Delta = 10^{-3}$ m. Similar to what happens with the parameter d, it was verified that for small values of k_i, the graph of the impact energy is very similar to the graph of impact energy with the same k_i and $\Delta = 0$ m. However, as k_i increases the form of the graph changes completely if compared to the graph of impact energy with the same k_i and $\Delta = 0$ m. It was also observed that the maximum of the impact energy do not occur anymore with the bigger k_i as happens in the $\Delta = 0$ m configuration. In the stochastic analysis, the stiffness of the spring k_i, in the barrier was modeled as a random variable and the propagation of uncertainties in the

coupled motor-cart-pendulum-barrier system was computed through Monte Carlo simulations. Thus statistics of the impact energy, as mean and 90% confidence interval, were computed for different values of gap$/l_p$, $E\{K_i\}$ and δ. Comparing these statistics with the results of deterministic simulations, it is verified that in relation to the mean of impact energy, deterministic and stochastic systems have similar behavior. However, the 90% confidence interval decreases as $E\{K_i\}$ increases and expands as δ increases.